International Journal of Thermofluids 5–6 (2020) 100038

Contents lists available at ScienceDirect

International Journal of Thermofluids

journal homepage: www.elsevier.com/locate/ijtf

Experimental investigation and analytical prediction of a multi-channel flat heat pipe thermal performance

Valentin Guichet, Navid Khordehgah, Hussam Jouhara*

Institute of Energy Futures, College of Engineering, Design and Physical Sciences, Brunel University London, UB8 3PH, UK

ARTICLE INFO

Article History:
Received 17 April 2020
Revised 19 June 2020
Accepted 6 July 2020
Available online 9 July 2020

Keywords:
Heat pipe
Multi-channel
Two-phase heat transfer
Modelling

ABSTRACT

Recently, multi-channel flat heat pipes have been developed to improve the heat recovery from flat surfaces, such as solar panels and batteries. In this paper, the thermal performance of a multi-channel flat heat pipe is experimentally investigated and analytically predicted. The multi-channel heat pipe studied transmits heat from silicone flat heaters to a water flow circulating inside a cooling manifold. The manifold heat sink is a flat aluminium surface comprising channels in which water recovers thermal energy by forced convection. The impact of the water flow rate on the working temperature of the heat pipe is investigated. To predict the performance and working temperature of the multi-channel flat heat pipe, a theoretical model has been developed. The thermal model considers the two-phase heat transfer in a multi-channel heat pipe geometry. It is shown that the heat pipe working temperature decreases with the water flow rate as a result of a reduced forced convection resistance of the manifold. Finally, the analytical multi-channel flat heat pipe model developed is compared with experimental data. It is shown that the thermal model, considering both cooling manifold and the multi-channel heat pipe geometry, is able to predict the heat pipe working temperature evolution within 7%.

1. Introduction

To transmit large amounts of thermal energy from small temperature gradients, heat pipes use the two-phase cycle of a working fluid to reach equivalent thermal conductivities of up to 100 kW/m.K [1]. These passive devices can be manufactured in various shapes to best fit their applications. As an example, circular heat pipes are commonly used in heat pipe-based heat exchangers (HPHE) in which heat is transmitted by forced convection from one fluid stream to another. More recently, industrialists and researchers have introduced multi-channel or multi leg heat pipes to extract thermal energy from flat surfaces. As witnessed by the work by Jouhara et al. [2], multi-channel heat pipes are also a promising solution to increase the heat transfer area between a flat heat source and the heat pipe itself. In this work [2], the multiple legs of the heat pipe permitted a more efficient heat recovery from a radiative source. Yet, this apparatus comprised cylindrical tubes which makes it more suitable for radiation but less suitable for surface cooling applications as the contact surface isn't rigorously flat. To cool down cylindrical batteries with heat pipes, Gan et al. [3] have used a conductive element that links the cylindrical batteries to heat pipes for which the evaporators are flattened. The heat pipe internal geometry comprised a single wicked cavity and all the heat pipes worked in parallel independently. Recently, heat pipes have been introduced to photovoltaic-thermal (PV/T) applications. Such modules have two main advantages: on the one hand, heat pipes prevent the photovoltaic cell surface from overheating which would decrease the electricity production of the cell; on the other hand, in addition to the enhanced electrical energy produced, heat pipes allow simultaneous thermal energy recovery. Gang et al. [4] were among the first researchers to use parallel circular heat pipes to recover thermal heat from photovoltaic cells. The potential of the author's idea was highlighted as their innovative system reached a thermal efficiency of 42%. However, due to the small contact area between the circular heat pipes and the flat PV cell, it appeared that the cooling of the photovoltaic cells wasn't optimum. Hu et al. [5] compared the thermal performances of two different PV/T systems, namely a wire-meshed heat pipe PV/T system and a wickless heat pipe PV/T system. In the two systems studied, the circular heat pipes are linked to an aluminium plate and to a cooling water pipe which significantly limits the contact area with the photovoltaic cells. Hu et al. [5] found that, unlike the wickless heat pipe-based PV/T system, the wire-meshed heat pipe-based PV/T system was not sensitive to inclination angle. The thermal efficiencies of the wire-meshed heat pipe-based PV/T prototype and of the wickless heat pipe-based PV/T system were 51.5% and 52.8%, respectively. Later, multi-channel heat pipes with flat surfaces have

* Corresponding author.
E-mail address: hussam.jouhara@brunel.ac.uk (H. Jouhara).

https://doi.org/10.1016/j.ijft.2020.100038

Nomenclature

A	surface area, m^2
C	constant, Dimensionless
c_p	specific heat, $J.kg^{-1}.K^{-1}$
C_{sf}	constant in Rohsenow correlation depending on the surface-fluid combination, Dimensionless
D	diameter, m
D_h	hydraulic diameter, m
f	friction factor, Dimensionless
g	gravitational acceleration, $m.s^{-2}$
h	heat transfer coefficient, $W.m^{-2}.K^{-1}$
i_{lv}	latent heat of vaporization, $J.kg^{-1}$
k	thermal conductivity, $W.m^{-1}.K^{-1}$
L	length, m
$\dot{m}$	mass flow rate, $kg.s^{-1}$
Nu	Nusselt number, Dimensionless
p	wetted perimeter, m
Pr	Prandtl number, ($Pr = c_p\mu/k$), Dimensionless
$\dot{Q}$	heat transfer rate, W
q''	heat flux per surface unit area, $W.m^{-2}$
R	thermal resistance, $K.W^{-1}$
Re	Reynolds number, ($Re = \rho vD/\mu$), Dimensionless
T	temperature, K
v	velocity, $m.s^{-1}$
w	pitch, m
z	thickness, m

Greek symbols

Δ	difference
ρ	density, $kg.m^{-3}$
σ	surface tension, $N.m^{-1}$
μ	dynamic viscosity, Pa.s

Subscripts

Alum	aluminium
boiling	boiling
c	condenser
condensation	condensation
e	evaporator
exp	experiment
fc	forced convection
h	hydraulic
in	inlet
l	liquid
LN	log mean temperature difference
manifold	cooling manifold
out	outlet
s	surface
th	theory
v	vapour
water	water

Superscripts

"	per surface area, m^{-2}
.	per unit of time, s^{-1}

Acronyms

Cond	condenser
Evap	evaporator
FR	filling ratio
HP	heat pipe
PKN	Prandtl–Karman–Nikuradse
PV/T	photovoltaic/Thermal

been developed for photovoltaic-thermal (PV/T) applications to increase the contact area between the cells and the heat pipe. Deng et al. [6] developed a micro-heat-pipe array as a photovoltaic-thermal module. The numerous micro heat pipe arrays used underneath the PV cells were placed in parallel and worked independently. Heat was then transmitted to a water flow through an air foil-shaped heat exchanger. The performance of the system was recorded for a year and the maximum combined efficiency reached 45.4%, including 13.4% electrical efficiency and 31.6% thermal efficiency. Yu et al. [7] experimentally investigated the performance of a solar micro-channel loop heat pipe used for PV/T application. In this system, the photovoltaic cells are placed on top of an aluminium plate which transmits thermal energy to twenty flat micro-heat pipes in parallel that contain micro-channels where the working fluid circulates. The system has the disadvantage of having an aluminium plate between the photovoltaic cell and the heat pipe which increases the conductive thermal resistance. In addition, the loop heat pipe is separated into twenty sections which decreases the contact surface area and limits the heat recovery from the hot surface to the heat pipe. Nevertheless, the system showed a maximum thermal efficiency of 62.2%. Jouhara et al. [8] invented a complex multi-channel flat heat pipe called “heat mat” that uses a unique internal multi-channel geometry to improve the thermal energy transmission from hot surfaces. The heat mat was tested as a PV/T system and reached thermal and electrical efficiencies of 64% and 6.1% respectively. It was also demonstrated that cooling the photovoltaic cell using the multi-channel flat heat pipe increases its efficiency by 15%. Multi-channel flat heat pipes are also particularly suitable for other applications that imply heat transfer from flat surfaces. For instance, Jouhara et al. [9] derived a similar multi-channel flat heat pipe (heat mat) as a battery cooling device to control and maintain the temperature of a battery within $\pm 1°C$. In this work, it is shown that the heat mat removed 60% of the generated heat from the battery while ensuring a uniform cooling due to the two-phase heat transfer. Shittu et al. [10] studied a micro-channel heat pipe based photovoltaic-thermoelectric system experimentally. In this design, the thermal energy extracted from the photovoltaic cells and transmitted through a flat heat pipe is reused to create more electricity by using a thermoelectric generator. From the Seebeck effect, the thermoelectric generator has the capacity to create electricity if the temperature of both side of the generator is different. By having, on the one hand, the flat heat pipe transmitting heat from the PV cell, and on the other hand, a water-cooled block, the part of the thermal energy conveyed by the flat heat pipe is further converted in electricity. This layout is advised for applications where electrical energy recovery is preferred to thermal energy. The maximum thermal efficiency of the system was 69.5%. However, in this work, the heat pipe structure and performance haven’t been investigated and detailed. Diao et al. [11] designed a new type of latent heat thermal energy storage device based on six parallel flat micro-heat pipe arrays. The heat transfer area inside the channels is increased as each channel comprises rectangular fins. The apparatus was studied experimentally and numerically using computational fluid dynamic technics but wasn’t modelled theoretically.

Indeed, in the current literature, the number of works reporting predictive analytical models for multi-channel heat pipes is poor. Up to date, studies such as the works by Payakaruk et al. [12], Shabgard et al. [13], Noie [14], and Guichet et al. [15,16] have proposed theoretical models of single cylindrical thermosyphons (wickless heat pipes) but no analytical model considering several parallel multi-channels linked at the top and bottom has been developed. Li et al. [17] experimentally studied the thermal performance of a novel thermal energy storage prototype which uses a flat micro-heat pipe array. However, the authors didn’t analyse their prototype with a theoretical approach. Delpech et al. [18] used a multi-leg heat pipe to extract

thermal energy from the radiation of ceramic tiles. The heat pipe was made of ten parallel tubes linked by top and bottom headers. An equivalent thermal resistance model has been proposed but not detailed. In this work [18], the heat pipe is considered as one entity and the influence of each leg hasn't been modelled. Similarly, Almahmoud and Jouhara [19] experimentally and theoretically investigated the performance of a radiative multi-channel heat pipe for waste heat recovery in the steel industry. The heat pipe consisted of fourteen stainless tubes connected by a collector at the bottom and by a shell and tube condenser at the top. A model including the radiative source, the heat pipe and the shell and tube condenser resistance have been developed. Yet, the internal model of the heat pipe considering the influence of the parallel tubes hasn't been reported.

Based on this state of the art, this work aims at developing an analytical model of a multi-channel flat heat pipe and the prediction of the thermal performance of the flat heat pipe and its cooling manifold. The developed model is then compared to experimental results in order to make conclusions about its capacity to predict the temperatures in the system and its accuracy.

2. Experimental setup

To investigate the two-phase heat transfer in a multi-channel flat heat pipe and validate the analytical model developed, the thermal performance of a flat heat pipe comprising parallel multi-channels is tested experimentally. The experimental test rig used for this investigation is presented in Fig. 1 hereafter.

At the evaporator section of the heat pipe, two flat silicone heaters generate heat which is transmitted to the multi-channel flat heat pipe. The thermal energy from the heaters is then conveyed by the heat pipe to the condenser section at the top. At the condenser section, a cooling manifold, in which cold water is circulating, is placed on the flat surface of the heat pipe and recovers heat. At the contact between the cooling manifold surface and the flat heat pipe, a high conductivity thermal paste was placed to improve the contact between the surfaces. Inside the cooling manifold, a water flow circulates through four consecutive passes in which each pass comprises several parallel channels. In the channels, water is progressively warming up and recovering thermal energy by forced convection. Inside the heat pipe, forty-three vertical parallel channels, linked at the top and bottom by horizontal collectors, transfer thermal energy by two-phase heat transfer. The unique shape of the channels and grooves inside the heat pipe was developed by Jouhara and Lester [20]. The internal structure of this unique heat pipe is described in the International Patent no WO2015193683 [20]. The channels' shape is included in a circle of approximately 6mm and the pitch between each channel is 11mm. In the cooling manifold, the channel geometry is identical to that of the heat pipe. The heat pipe working fluid used in the multi-channel flat heat pipe is ammonia and in terms of the volume of the evaporator section, the filling ratio is 100%. Ammonia was chosen as a working fluid due to its high figure of merit in the considered working temperatures, material compatibility with aluminium, and limited environmental impact when compared to commercially compatible refrigerants. Both cooling manifold and heat pipe are manufactured in aluminium and the whole system has been covered by insulation to limit the heat losses to the environment. At the evaporator, the heaters are controlled by a PID (proportional integral derivative) controller in which the feedback temperature is measured at the surface of the heaters. The choice of using a PID controller was justified in the objective of maintaining a constant evaporator surface temperature between all the experiments. During the experiments, the heat transfer rate in the system was experimentally measured to be around 500W as heat losses occurred. Yet, an observed limit of using a PID controller is the possibility of slightly changing the heat transfer rate if the heat pipe surface temperature decreases with an increased water flow rate. To change the water flow inside the manifold, a valve is used, and the flow is measured by a flow meter OMEGA Turbine flow sensor FTB370 with an error estimated at 5%. The experimental set-up and its piping and instrumentation diagram are presented in Figs. 2 and 3.

To measure the water flow and heat pipe temperatures, K-type thermocouples have been used. These thermocouples are suitable for a temperature range between -40°C to 1110°C and their measurement error is estimated to be ±0.25°C. Two thermocouples have been used to measure the water temperature before and after the cooling manifold, whereas fourteen thermocouples have been placed on the system to characterize the thermal behaviour of the prototype. The location of the thermocouples in the system and their designation are detailed in Fig. 4 below.

At the evaporator section, the thermocouples LT5 and RT5 are placed on the top of the heaters. Along the heat pipe surface, the thermocouples RT2, RT3, RT4, LT3, and LT4 have been placed at the front of the heat pipe surface to measure the temperature at multiple location of the adiabatic section. At the condenser section, the

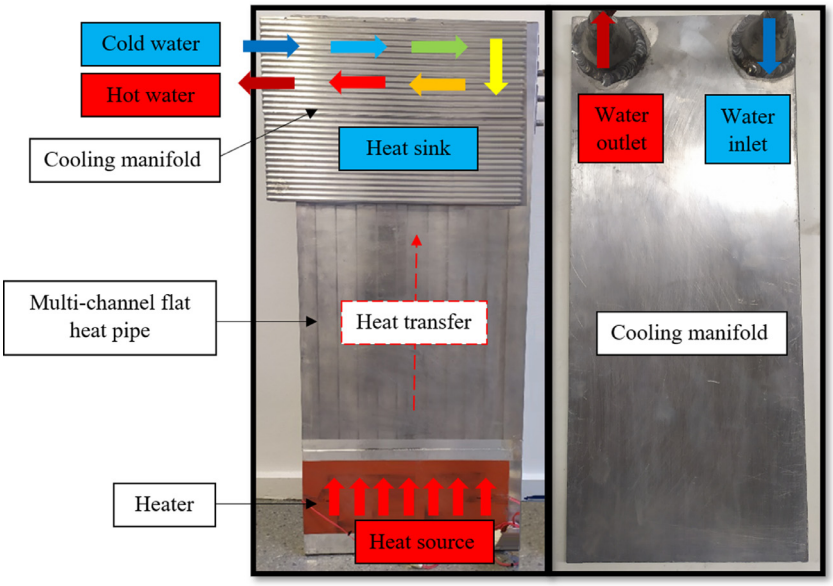

Fig. 1. Experimental set-up of the multi-channel flat heat pipe and its cooling manifold.

Fig. 2. Experimental set-up.

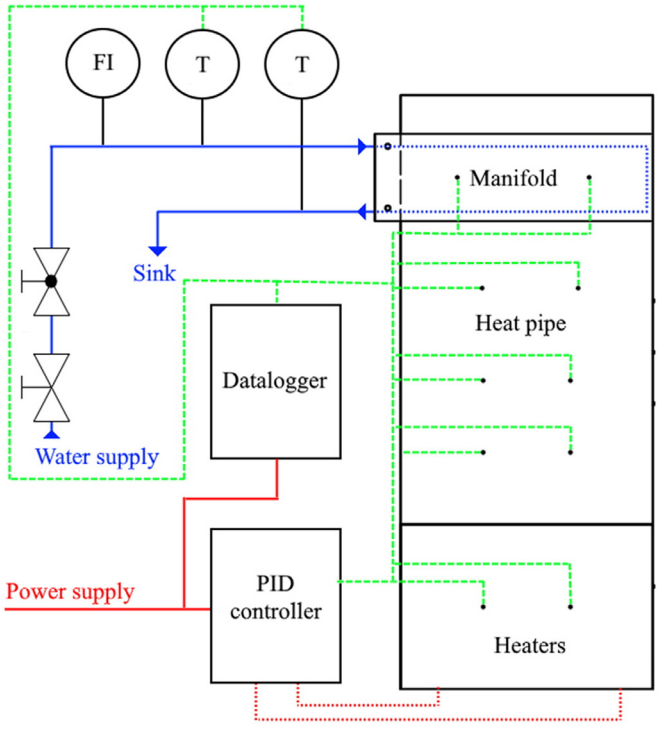

Fig. 3. Piping and instrumentation diagram (P&ID) of the system.

thermocouple RT1 is placed between the heat pipe surface and the cooling manifold interface. To compare the heat pipe condenser temperature with that of the cooling manifold, a thermocouple LT1 has been placed on the top of the cooling manifold, on the surface which is not in contact with the heat pipe. Finally, the thermocouples SD1, SD2 and SD4 are placed on the back surface of the heat pipe. To limit the influence of the surrounding on the temperature sensors, a thermal paste is used to increase the thermal conductivity at the contact. Furthermore, the thermocouples are fixed to the surfaces with a layer of thermal insulation to guarantee the thermocouple is at the same temperature as the surface and increase the precision of the temperature readings. The sensor readings are collected and recorded with a NI USB-9162 portable data logger. The errors conveyed by the data logger itself are assumed very small and negligible compared to the measurement errors.

3. Theory and analytical modelling

3.1. Theoretical background

In the objective of modelling the cooling manifold, forced convection correlations must be used. As an increase of turbulence leads to a better mixing of the flow and thus increases the heat transfer, forced convection heat transfer correlations vary according to the Reynolds number Re of the flow defined by:

$$Re = \frac{\rho_{water} v_m D_h}{\mu_{water}} \tag{1}$$

with ρ_{water} the density of water (kg/m3), v_m the mean velocity of water inside the tube (m/s), D_h the hydraulic diameter of the section (m), and μ_{water} the dynamic viscosity of water (Pa.s). The mean velocity of the flow can be obtained with:

$$v_m = \frac{\dot{m}}{\rho_{water} A_{cross\text{-}section}} \tag{2}$$

where $\dot{m}$ is the water mass flow rate (kg/s), ρ_{water} is the density of water (kg/m^3), and $A_{cross\text{-}section}$ the cross-section surface area. The flow regimes of a fluid is commonly described according to the following limits [1,21,22]:

$$\begin{array}{l} Re < 2300 \text{ Laminar flow} \\ 2300 \leq Re \leq 10000 \text{ Transitional flow} \\ 10000 \leq Re \text{ Turbulent flow} \end{array} \tag{3}$$

To determine the forced convection heat transfer coefficient in the cooling manifold, according to the regime of the water flow in the channels, different correlations are used. Among the forced convection heat transfer correlations reported in the literature, many use the friction factor f to describe the wall-fluid interaction. Obviously, the friction of the water flow on the wall also depends on the flow regime and therefore are correlated in terms of Reynolds number. A state of the art of friction factor f correlations for smooth circular tubes is presented by Cengel [1] and Rohsenow [22]. Among the available friction factor equation, the correlation by Prandtl et al. [23] can be used to describe turbulent flows ($4.e^{-3} \leq Re \leq 1.e^{-7}$):

$$\frac{1}{\sqrt{f}} = 1.7272 \times ln\left(Re\sqrt{f}\right) - 0.3946 \tag{4}$$

The correlation by Prandtl et al. [23], sometimes designated by "PKN" in reference to Prandtl–Karman–Nikuradse, is often considered as the most accurate correlation. However, this correlation cannot easily be solved and gives implicit values of the frictional factor. Therefore, to estimate the friction factor, other explicit formulas are commonly used. According to the literature, the estimation of the friction factor is quite accurate and discrepancies between experimental and theoretical values are typically in the range of 5% [22]. However, the estimation of the forced convection heat transfer coefficient is more difficult and most of the reported correlations have an accuracy limited to 20%. This accuracy is even more degraded in the transitional region where the flow randomly switches between the laminar and turbulent regime. To estimate the forced convection heat transfer

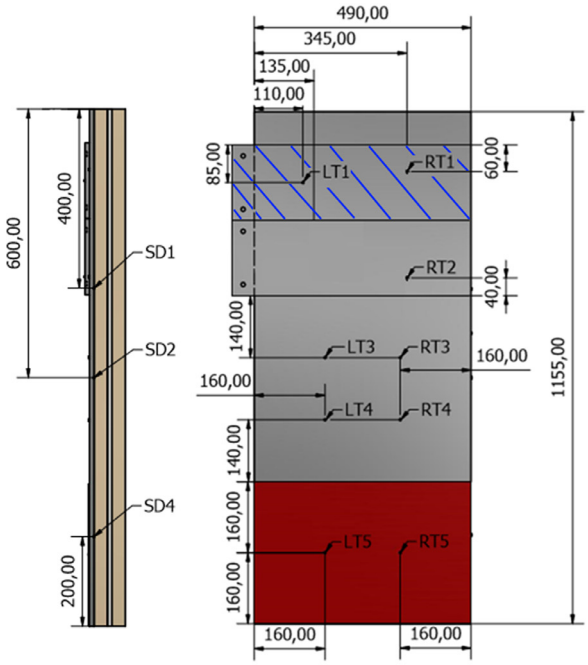

Designation	Location
LT1	Cooling manifold surface
RT1	Condenser section, Front HP surface
RT2	Adiabatic section, Front HP surface
SD1, SD2	Adiabatic section, Back HP surface
LT3, RT3	Adiabatic section, Front HP surface
LT4, RT4	Adabatic section, Front HP surface
SD4	Evaporator, Back HP surface
LT5, RT5	Heater surface

Fig. 4. Thermocouples designation and location.

coefficient inside a tube, correlations are commonly reported in terms of Nusselt number *Nu*:

$$Nu = \frac{hD}{k} \tag{5}$$

where h is the forced convection heat transfer coefficient (W/m^2.K), D is the tube diameter (m), and k is the fluid thermal conductivity (W/m.K). A state of the art of reported internal forced convection heat transfer coefficient in smooth tubes is available from Cengel [1] and Rohsenow [22]. In this study, most of the water flow Reynolds numbers in the cooling manifold belong to the transitional regime. Due to the relatively low number of internal forced convection correlations developed for transitional flow only, and on the difficulty of researchers to describe this regime, several correlations have been tested.

3.2. Thermal model of the complete system

To investigate the two-phase heat transfer in the multi-channel flat heat pipe, a thermal model of the complete system must be made. The model takes into account the heat source represented by the electrical heaters, the multi-channel flat heat pipe, and the heat sink represented by the cooling manifold. Even if the focus and novelty of this work is the investigation of the multi-channel flat heat pipe thermal behaviour, the analytical model needs to include the cooling manifold to perform an energy balance on the heat transfer rate in the system. The equivalent thermal resistance model of the complete system including the heat source, the heat pipe and the cooling manifold resistance is presented in Fig. 5.

The different resistances presented in the above model are detailed in Table 1 hereafter:

3.3. Cooling manifold model

This section focuses on modelling the cooling manifold which is used as a heat sink. At the top of the heat pipe the flat manifold recovers the heat transmitted by the multi-channel flat heat pipe. Inside the manifold, cold water is circulating through fifteen channels. The channels are linked at the extremities by grooves to form a total of four passes. The geometrical characteristics of the cooling manifold considered in the model are detailed in Table 2 hereafter.

Due to the complex cross-sectional geometry of the channels, these are simulated by tubes contained in a solid material with a hydraulic diameter defined by [22]:

$$D_h = \frac{4A_c}{p} \tag{6}$$

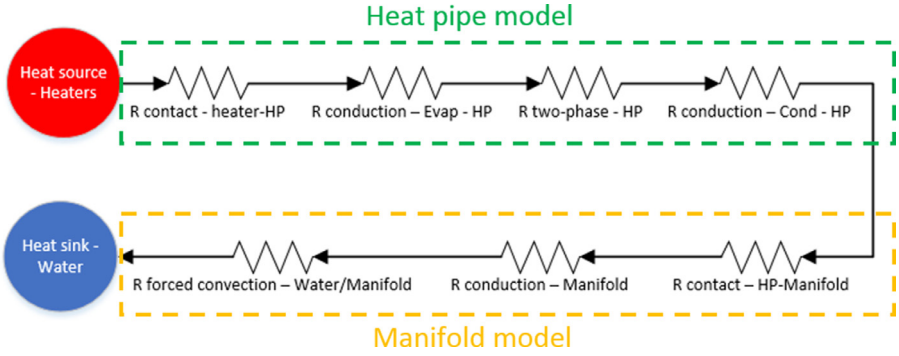

Fig. 5. Complete thermal resistance model of the system considered.

Table 1
Thermal resistances considered in the model.

Resistance	Physical meaning
R contact – heater - HP	Surface resistance at the contact between the heaters and the heat pipe
R conduction – Evap - HP	Conduction resistance through the heat pipe thickness to the working fluid at the evaporator
R two-phase - HP	Two-phase resistance of the working fluid inside the heat pipe
R conduction – Cond – HP	Conduction resistance through the heat pipe thickness to the surface of the heat pipe at the condenser
R contact – HP - Manifold	Surface resistance at the contact between the heat pipe and the manifold
R conduction - Manifold	Conduction resistance through the manifold thickness to the inner channels' walls.
R forced convection – Water/ Manifold	Forced convection of the water circulating inside the heated walls of the manifold

Table 2
Geometrical characteristics of the cooling manifold considered in the model.

Geometry	Characteristics
Manifold outside surface dimensions	177 × 400 mm
Number of passes	4
Number of channels	15
Number of channels per passes	Pass 1,2,3: 4 channels; Pass 4: 3 channels
Pitch between the channels	11 mm
Length of channels	386 mm
Length of the grooves	Groove 1: 75 mm; Grooves 2,3: 85 mm
Hydraulic diameter of a channel	3.27 mm
Diameter of the grooves	6 mm

where the hydraulic diameter D_h (m) is a function of the cross-sectional area A_c of the channel (m^2) and of the wetted perimeter p (m).

In the manifold, heat is received by the flat heat pipe surface. As discussed in the next section dealing with the heat pipe model, the heat pipe surface temperature is assumed homogeneous as condensation takes place in the multi-channel geometry. Furthermore, the four passes of the cooling manifold balance the temperature differences along a single channel. In this regard, the temperature profile of the manifold hot surface is also considered uniform in this model.

Inside the manifold, water is circulating through four consecutive passes. The three first passes are made of four parallel channels while the last pass comprises three parallel channels only, for a total of fifteen channels. Hence, the equivalent thermal model first considers that heat is transmitted by conduction to each channel, and second, that this heat is then recovered by the water flow by forced convection through the channels. The equivalent thermal resistance model of the cooling manifold developed is presented in Fig. 6.

In the model, the hot manifold surface in contact with the heat pipe is represented by a red oval at a temperature $T_{man,\ out}$. For each channel, an equivalent resistance of conduction describes the conduction heat transfer through the manifold thickness while the forced convection resistance estimates the heat transfer between the hot wall of the channel and the water flow. As the temperature is considered uniform at the outside surface of the manifold in contact with the heat pipe and because the thermal conductivity of aluminium is relatively high, the model considers that the temperature of the channel walls is similar for the parallel channels.

To estimate the thermal resistance of each channel, the parallel arrangement of the channels is considered by using a conduction shape factor according to the internal geometry of the cooling manifold. Then, the conduction resistance for each channel is estimated using [1]:

$$R_{conduction-\ 1\ channel} = \frac{\ln\left(\frac{2w}{\pi D_h} sinh\frac{2\pi z}{w}\right)}{k_{alum} 2\pi L} \quad (for\ each\ channel) \tag{7}$$

with w the pitch between each parallel channel (m), D_h the hydraulic diameter of the channels (m), z the material thickness between the hot surface and the channels (m), L the length of the channels (m), and k_{alum} the thermal conductivity of the aluminium wall (W/m.K). The forced convection resistance of a channel is given by [22]:

$$R_{forced\ conv-channel} = \frac{1}{h_{fc} A_{fc,\ channel}} \quad (for\ each\ channel) \tag{8}$$

where h_{fc} is the forced convection heat transfer coefficient ($W/m^2.K$), and $A_{fc,channel}$ the forced convection area in the channel (m^2). A similar formula can be used to estimate the forced convection resistance inside the grooves between each pass. To estimate the forced convection heat transfer coefficient, numerous arrangements of correlations for both friction factor and Nusselt number have been tested. Due to the transitional nature of the flow, many have been found unsuitable to predict the thermal behaviour of the cooling manifold. In addition, the unique internal shape of the channels plays a significant role in the flow distribution and turbulence in a channel which is not considered when approximating a channel as a tube by its hydraulic diameter. According to these particular considerations, after testing several reported model, the best fitting correlation to estimate the transitional forced convection heat transfer coefficient in the cooling manifold was developed by Edwards et al. [24]:

$$Nu = \frac{h_{fc} D_h}{k_{water}} = 3.66 + \frac{0.065(D_h/L)RePr}{1 + 0.04[(D_h/L)RePr]^{2/3}} \tag{9}$$

where h_{fc} is the forced convection heat transfer coefficient ($W/m^2.K$), D_h the hydraulic diameter of the channels (m), k_{water} the thermal conductivity of the water (W/m.K), L the length of the channel (m), Re the flow Reynolds number, and Pr the water flow Prandtl number is given by:

$$Pr = \frac{c_p \mu}{k} \tag{10}$$

where c_p is the water specific heat (J/kg.K), μ the water dynamic viscosity (Pa.s), and k the water thermal conductivity (W/m.K). As the water properties vary with the temperature, the thermal model automatically estimates the properties at the average temperature between the inlet and outlet of the manifold.

3.4. Multi-channel heat pipe model

The focus of this work is to develop a theoretical model of the multi-channel flat heat pipe. In the case studied, the heat pipe receives thermal energy by contact with electrical heaters at the bottom (evaporator section), transports the heat by two-phase heat transfer in the multi-channels, and finally releases its energy by condensation at the contact with the cold cooling manifold wall (condenser section). The heat pipe studied comprises 43 vertical channels linked at the top and bottom by horizontal collectors. The horizontal collectors aim at bringing a homogeneity of the two-phase flow and allow a communication of all the parallel vertical channels. The internal geometry of the multi-channel flat heat pipe is detailed in the International Patent n° WO2015193683 [20] and is schematized in Fig. 7.

To predict the multi-channel flat heat pipe performance and working temperature, an equivalent thermal resistance model of a multi-channel flat heat pipe has been developed and is presented in Fig. 8.

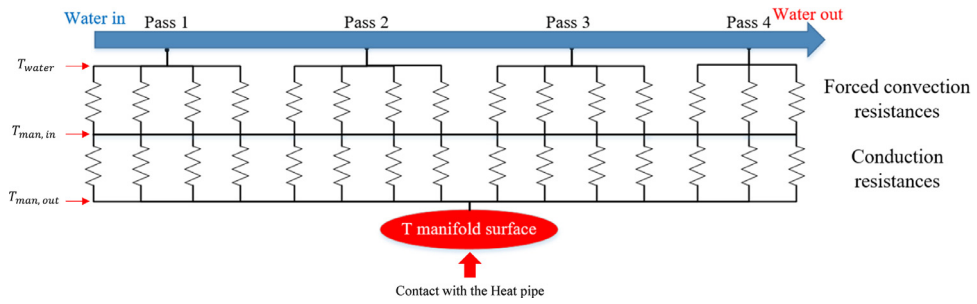

Fig. 6. Cooling manifold thermal resistance model.

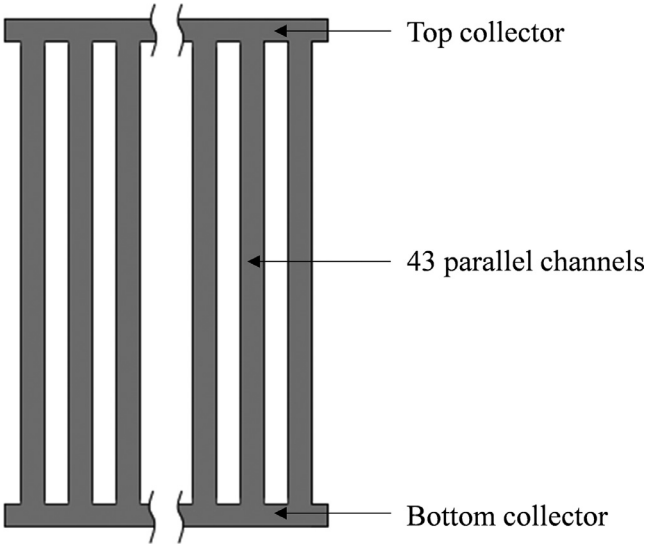

Fig. 7. Schematized internal geometry of the multi-channel flat heat pipe.

In this model, two types of channels must be considered: while the vertical channels are similar and assumed to have the same thermal resistance, the horizontal collectors that link the channels at the top and at the bottom are also included. These must be differentiated as the collectors do not have a similar geometry as the parallel channels. Inside the multi-channel heat pipe, the top and bottom aim at maintaining the homogeneity of the two-phase flow and limit local saturation temperature differences.

In the model, the wall resistances represent the conduction resistances through the thickness of the heat pipe at the evaporator (subscript e) and at the condenser (subscript c). At the contact with the heat source, the working fluid inside the manifold boils at the evaporator. Two-different two-phase mechanisms are taking place in the channels: At the bottom of the channels, pool boiling occurs whereas, on the wall, the condensate that returns to the pool also evaporates. This is often designated as falling film boiling. In the channels, these two phenomena, namely pool boiling and falling film boiling, work simultaneously in parallel, depending on the working fluid filling ratio (ratio between the volume of working fluid in the heat pipe and volume of the evaporator). In the case studied, the filling ratio of the heat pipe was high enough so that the evaporator volume was filled by the liquid pool. Hence, in this special configuration, pool boiling only was considered.

To estimate the conduction through the heat pipe thickness to each channel, a conduction shape factor is used. This factor has been developed to consider the conduction heat transfer from a surface to parallel cylinders inside the material thickness. The geometry considered is illustrated in Fig. 9 [1].

Similarly to the cooling manifold, the conduction resistance through the thickness of the heat pipe is estimated using the shape factor S given by [1]:

$$S = \frac{2\pi L}{\ln\left(\frac{2w}{\pi D}\sinh\frac{2\pi z}{w}\right)} \quad (for\ each\ channel) \tag{11}$$

With L the length of the channels (m), w the pitch between the channels (m), z the material thickness between the heat pipe surface and the channels (m), and D the diameter of the channels (m). In the case studied, the hydraulic diameter of the channels is used. Then, for each channel, the conduction thermal resistance is given by [1]:

$$R_{conduction-\,1\ channel} = \frac{1}{k_{alum}S} = \frac{\ln\left(\frac{2w}{\pi D}\sinh\frac{2\pi z}{w}\right)}{k_{alum}2\pi L} \quad (for\ each\ channel) \tag{12}$$

with k_{alum} the thermal conductivity of aluminium (W/m.K), and the geometrical parameters given as per Fig. 9. To estimate the overall conduction resistance, the parallel channel resistances must be summed according to the equivalent resistance rules.

To estimate the boiling and condensation thermal resistances in the multi-channel heat pipe, correlations must be used to estimate the boiling and condensation heat transfer coefficients. Then, the thermal resistance can be retrieved from:

$$R_{boiling/condensation} = \frac{1}{h_{boiling/condensation}A_{boiling/condensation}} \tag{13}$$

with $R_{boiling/condensation}$ the boiling/condensation thermal resistance (K/W), $h_{boiling/condensation}$ the boiling/condensation heat transfer coefficient (W/m^{2}K), and $A_{boiling/condensation}$ the corresponding heat transfer area (m^2). To estimate the pool boiling heat transfer coefficient, one of the most recommended correlations [15] was developed by *Rohsenow* [25]:

$$h_{boiling} = \left(\frac{q''_{boiling}}{i_{lv}}\right)^{1-r}\left[\mu_l/\sqrt{\frac{\sigma}{g(\rho_l-\rho_v)}}\right]^{r}\frac{c_{p,l}}{C_{sf}}Pr_l^{-s} \tag{14}$$

v $r = 1/3$
v $\{s = n = 1$ *for water* $s = n = 1.7$ *for other fluids*

with $q''_{boiling}$ the heat flux (W/m^2), i_{lv} the latent heat of vaporization (J/kg), μ_l the liquid dynamic viscosity (kg/m.s), σ the liquid surface tension (N/m), g the gravitational acceleration (m/s^2), ρ_l and ρ_v the density of the liquid and vapour phases respectively (kg/m^3), $c_{p,l}$ the specific heat of the liquid (J/kg.K), and Pr_l=$\mu c_p/k$ the Prandtl number of the liquid. The constant C_{sf} depends on the solid/fluid characteristics. For aluminium/ammonia characteristics, the constant C_{sf} has been taken as C_{sf}=0.013 [22].

Similarly, the condensation heat transfer coefficient can be estimated using the correlation by *Nusselt* [26] which is widely advised in the literature [16]:

$$h_{condensation} = 0.943\left\{\frac{\rho_l(\rho_l-\rho_v)i_{lv}gk_l^{\,3}}{\mu_l L_c(T_{sat}-T_w)}\right\}^{1/4} \tag{15}$$

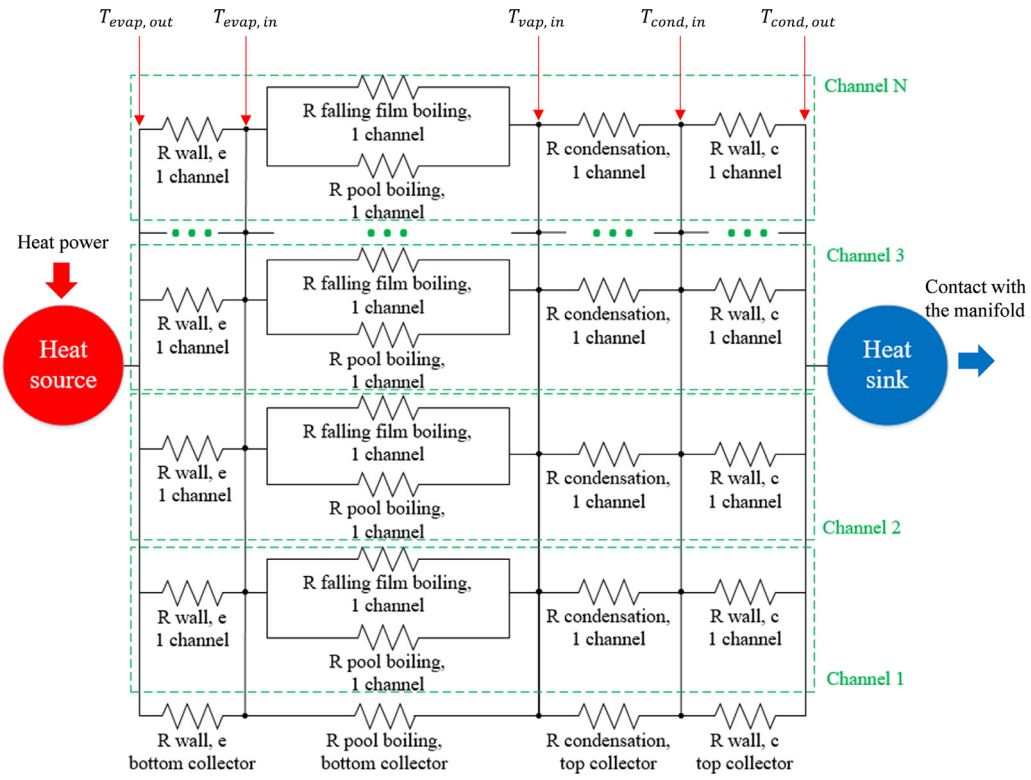

Fig. 8. Multi-channel flat heat pipe thermal resistance model considered.

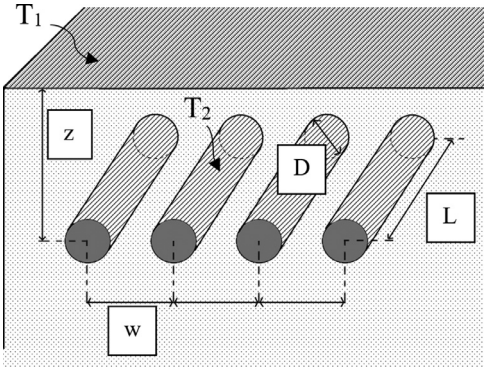

Fig. 9. Conduction geometry considered by the shape factor, adapted from Cengel [15].

with k_l the liquid thermal conductivity (W/m.K), L_c the condenser length (m), T_{sat} the saturation temperature (K), and T_w the wall temperature (K). The above correlations have been used to model the multi-channel flat heat pipe as per Fig. 8.

3.5. Energy balance and iterative method

Based on the cooling manifold and multi-channel flat heat pipe models previously described, an iterative tool has been built using Excel and VBA coding. Indeed, the prediction of the temperatures inside the system cannot be estimated directly and iterations are needed. In the studied system, the heat transfer rate is estimated by measuring the electrical consumption and estimating the heat losses. Then, according to the first principle of thermodynamics, the heat transfer rate provided to the system is recovered by the water flow in the cooling manifold:

$$\dot{Q}_{provided} = \dot{Q}_{water} = \dot{m}_{water} c_{p,water} \Delta T_{water} \tag{16}$$

where $\dot{Q}$ is the heat transfer rate through the system (W), $\dot{m}_{water}$ is the water flow rate in the cooling manifold (kg/s), $c_{p,water}$ is the specific heat of water (J/kg.K), and ΔT_{water} is the temperature difference in the water flow (K). By assuming the evaporator temperature of the heat pipe, the tool evaluates the different thermal resistances and calculates the temperatures in the system. Then, according to heat exchanger theory, the temperatures of the system are linked to the water temperature by the logarithmic mean temperature difference (LMTD) given by:

$$\begin{aligned}\dot{Q}_{tot} &= \frac{1}{R_{manifold}} \Delta T_{LN} \\ &= \frac{1}{R_{manifold}} \times \frac{T_{water-in} - T_{water-out}}{ln((T_s - T_{water-out})/(T_s - T_{water-in}))}\end{aligned} \tag{17}$$

where $\dot{Q}_{tot}$ is the total heat transfer rate through the system (W), $R_{manifold}$ is the cooling manifold thermal resistance (K/W), $T_{water-in}$ and $T_{water-out}$ are the water inlet and outlet temperatures (K), and T_s is the surface temperature of the heat pipe in contact with the cooling manifold (K). The surface temperature of the heat pipe is estimated at each iteration using the multi-channel flat heat pipe model presented. By definition, the heat transfer rate through the system must be equal to the heat transfer rate recovered by the water flow. Therefore, the iterative model is used to change the evaporator temperature and the temperatures in the system until the following criterion is reached:

$$\dot{Q}_{water} = \dot{Q}_{tot} \tag{18}$$

4. Data reduction and error propagation

4.1. Measurement error

During the data analysis, errors can propagate through many factors such as human error, protocol followed, equipment used, etc. To characterize the accuracy of the measurement and thus of the results, an error

analysis is expected. In the analysis presented, three main sources of errors can be identified through the experimental process: thermocouple measurement error, water flow meter error, and data logger error. The thermocouples used are K-type thermocouples suitable for a temperature range between -40°C to 1110°C whose measurement error is estimated at ±0.25°C. The water flow rate was measured using an OMEGA Turbine flow sensor FTB370 series whose error is estimated of 5%. The sensors reading are collected and recorded with a NI USB-9162 portable data logger. The errors conveyed by the data logger by itself are assumed very small and negligible compared to the measurement errors. The measurement errors are summed up in Table 3.

4.2. Error propagation in the experimental multi-channel flat heat pipe thermal resistance

The experimental thermal resistance of the multi-channel flat heat pipe is estimated using:

$$R_{HP} = \frac{(T_{evaporator} - T_{condenser})}{\dot{Q}_{water}} \tag{19}$$

where R_{HP} is the experimental heat pipe thermal resistance (K/W), $T_{evaporator}$ and $T_{condenser}$ the evaporator and condenser temperatures (K), $\dot{m}_{water}$ the water flow rate in the cooling manifold (kg/s), $c_{p,water}$ the specific heat of water (J/kg.K), and ΔT_{water} is the temperature difference in the water flow (K). The error made on the heat transfer rate measurement $\sigma_{\dot{Q}_{water}}$ is obtained by:

$$\sigma_{\dot{Q}_{water}} = \dot{Q}_{water}\sqrt{\left(\frac{\sigma_{\dot{m}_{water}}}{\dot{m}_{water}}\right)^2 + \left(\frac{\sigma_{(T_{water-out}-T_{water-in})}}{(T_{water-out}-T_{water-in})}\right)^2} \tag{20}$$

with,

$$\sigma_{(T_{water-out}-T_{water-in})} = \sqrt{2}\sigma_T \tag{21}$$

where $\dot{m}_{water}$ is the water flow rate in the cooling manifold (kg/s), $T_{water-in}$ and $T_{water-out}$ are the water inlet and outlet temperatures (K), and σ is the associated absolute error. As the temperature measurements have a similar uncertainty, this error is designated by σ_T. From the above expressions, the error propagation made on the experimental thermal resistance of the multi-channel flat heat pipe is:

$$\sigma_{R_{HP}} = R_{HP}\sqrt{\left(\frac{\sigma_{(T_{evaporator}-T_{condenser})}}{(T_{evaporator}-T_{condenser})}\right)^2 + \left(\frac{\sigma_{\dot{Q}_{water}}}{\dot{Q}_{water}}\right)^2} \tag{22}$$

Based on this analysis, the estimated error propagated to the experimental heat pipe thermal resistance is presented in Table 4.

Another important factor that isn't considered in the error analysis is the location of the thermocouples. In particular, to estimate the evaporator temperature, the thermocouple was placed at the back of the multi-channel flat heat pipe as the electrical heaters were covering the front. This may have ended in an underestimation of the evaporator temperature.

4.3. Error propagation in the experimental cooling manifold thermal resistance

In the theoretical and experimental estimation of the cooling manifold resistances, errors have been conveyed from the measurement error, but also from the forced convection correlation used. The accuracy of the theoretical thermal model developed is highly linked to the accuracy of the forced convection correlation as the accuracy of such correlations, especially in the transitional regime, can lead to errors of 20% in the estimation of the forced convection heat transfer coefficient. Therefore, it is valuable to estimate the inaccuracy of the correlation used to balance it with the overall thermal model error. To estimate the error of the forced convection correlation from Edwards et al. [24], the experimental forced convection heat transfer coefficient in the first pass is compared with the correlation estimation based on the experimental measurements. This analysis is showed in Fig. 10.

The maximum error made by the forced convection correlation from Edwards et al. [24] when estimating the heat transfer coefficient is 11.4% and was obtained for a minimum water flow rate.

The equations used to estimate the experimental resistance of the manifold are listed hereafter:

$$R_{manifold} = \frac{1}{\dot{Q}_{water}} \times \frac{T_{water-in} - T_{water-out}}{ln((T_s - T_{water-out})/(T_s - T_{water-in}))} \tag{23}$$

$$\dot{Q}_{water} = \dot{m}_{water} c_{p,\ water} \Delta T_{water} \tag{24}$$

$$\dot{m}_{water} = \rho_{water} \times \left(\frac{\dot{V}_{water}}{60000}\right) \tag{25}$$

with $\dot{Q}_{water}$ the heat transfer rate recovered by the water (W), $T_{water-in}$ and $T_{water-out}$ the water inlet and outlet temperature (K), T_s the surface temperature at the between the heat pipe and the cooling manifold (K), $\dot{m}_{water}$ the water mass flow rate (kg/s), ρ_{water} the density of water (kg/m^3), and $\dot{V}_{water}$ the water flow rate (L/min). The error propagated to the experimental estimation of the cooling manifold resistance is given by:

$$\sigma_{R_{manifold}} = R_{manifold}\sqrt{\left(\frac{\sigma\{\Delta T_{water}\}}{\Delta T_{water}}\right)^2 + \left(\frac{\sigma\{\dot{Q}_{water}\}}{\dot{Q}_{water}}\right)^2 + \left(\frac{\sigma\{ln(C)\}}{ln(C)}\right)^2} \tag{26}$$

$$C = (T_s - T_{water-out})/(T_s - T_{water-in}) \tag{26}$$

$$\sigma\{\Delta T_{water}\} = \sqrt{2}\sigma_T \tag{27}$$

and the error made on the heat transfer rate recovered by the water $\sigma_{\dot{Q}_{water}}$ is given by Eq. (20). The error made on the logarithm is estimated using:

$$\sigma\{ln(C)\} = \sigma\left\{\left(\frac{T_s - T_{water-out}}{T_s - T_{water-in}}\right)\right\} \Big/ \left(\frac{T_s - T_{water-out}}{T_s - T_{water-in}}\right) \tag{29}$$

and,

$$\sigma\left\{\left(\frac{T_s - T_{water-out}}{T_s - T_{water-in}}\right)\right\} = \left(\frac{T_s - T_{water-out}}{T_s - T_{water-in}}\right)\sqrt{\left(\frac{\sigma\{T_s - T_{water-out}\}}{T_s - T_{water-out}}\right)^2 + \left(\frac{\sigma\{T_s - T_{water-in}\}}{T_s - T_{water-in}}\right)^2} \tag{30}$$

Table 3
Measurement error.

Equipment	Error
K-type thermocouple -40°C to 1110°C	± 0.25°C
OMEGA Turbine flow sensor FTB370 series	5%
NI USB-9162 portable data logger	Assumed negligible

Table 4
Measurement error propagation to the experimental heat pipe thermal resistance.

Water flow rate (kg/s)	0.07	0.10	0.14
Experimental heat pipe resistance (K/W)	0.0041	0.0040	0.0041
Absolute error (K/W)	0,0011	0,0013	0,0016
Relative error (%)	27.5 %	32.0 %	38.8 %

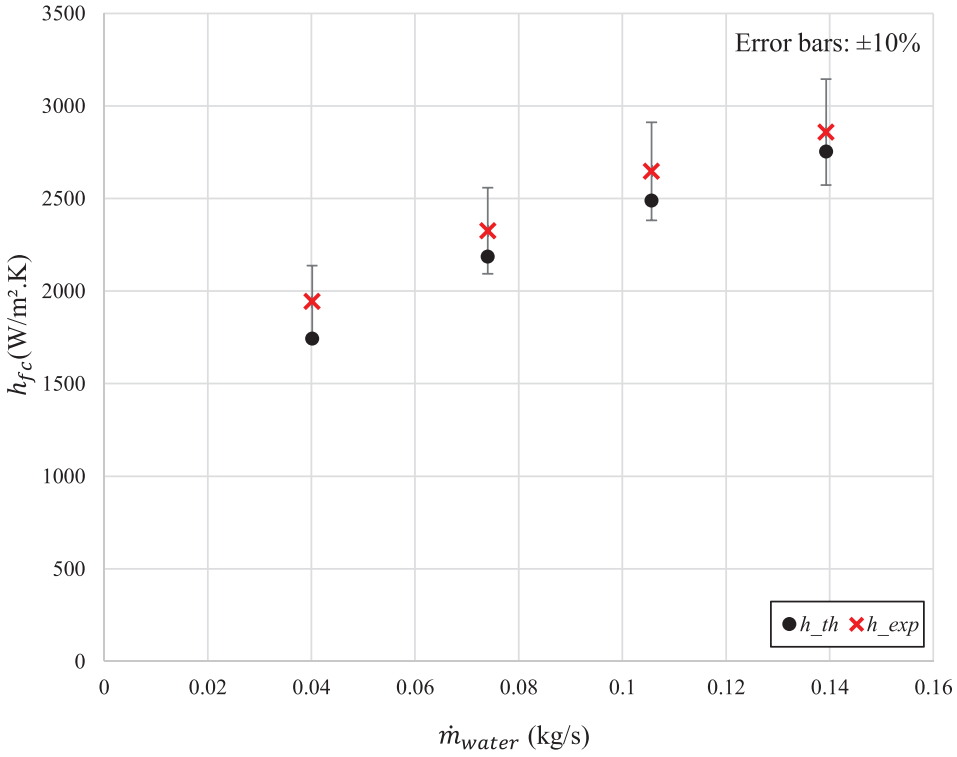

Fig. 10. Error analysis – accuracy of the forced convection correlation used.

with,

$$\sigma\{T_s - T_{water-out}\} = \sigma\{T_s - T_{water-in}\} = \sqrt{2}\sigma_T \quad (31)$$

The numerical analysis of the error propagation made in the estimation of the thermal resistance of the manifold is presented in Table 5.

Based on the estimation of the sensor's accuracy, the error made on the cooling manifold resistance estimation can be significant due to the very small values of thermal resistances studied and mainly due to high temperature measurement's inaccuracy compared to the difference of temperature in the system.

5. Results and discussion

5.1. Cooling manifold

The multi-channel flat heat pipe and its cooling manifold receive thermal energy which is transmitted by two silicone heaters. The heat transfer rate through the system is measure in two ways. At first, the electrical consumption allows an estimation of the energy provided by the system. Second, the heat transfer is measured experimentally and estimated using Eq. (16). As can be seen from Fig. 10, heat losses take place and the measured heat transfer rate is about 20% lower than the heat transfer rate estimated by measuring the electrical consumption. To consider the heat losses in the theoretical estimation by the model, the heat transfer rate estimated by the electrical consumption has been corrected. This analysis is presented in Fig. 11.

Table 5
Measurement error propagation to the experimental cooling manifold thermal resistance.

Water flow rate (kg/s)	0.04	0.07	0.11	0.14
Experimental heat pipe resistance (K/W)	0.0083	0.0069	0.0061	0.0056
Absolute error (K/W)	0.0024	0.0031	0.0034	0.0040
Relative error (%)	29%	44%	57%	72%

From the corrected estimation of the rate of heat transfer and using the water inlet temperature as a second input, the water outlet temperature in the cooling manifold is estimated using Eq. (16). In Fig. 12, the experimental and theoretical inlet and outlet water temperatures at the cooling manifold are presented. The accuracy of the model predictions for the water outlet temperature are directly linked to the accuracy of the estimation of heat transfer rate. It is verified that for the same heat transfer rate through the system, an increase in the water flow rate decreases the difference of temperature between the inlet and outlet. By comparing Figs. 11 and 12, it can be noted that the experimental measurements of the heat transfer rate are less accurate than the absolute temperature ones.

Based on the cooling manifold thermal model presented earlier, the manifold thermal resistance is predicted theoretically and varies according to the water flow rate. The comparison between experimental data and theoretical prediction of the cooling manifold thermal resistance is presented in Fig. 13. By increasing the water flow rate, the turbulence inside the manifold is increased which leads to an increase in the forced convection heat transfer coefficient. Hence, the overall thermal resistance of the cooling manifold reduces with an increase of the water flow rate. It is also observed that the model predictions are becoming more accurate with an increase in the water flow rate. Indeed, for a water flow rate of 0.04 kg/s, the error made on the prediction is 11.4% whereas at a water flow rate of 0.14 kg/s, this error falls to 3.8%. The improvement in the model prediction at higher flow rates is explained as a more turbulent flow is better described by the forced convection correlations reported in the literature, in comparison with transitional flow. The errors made in the predictions for the four tested flow rates are showed in Fig. 14. The developed theoretical model predicted the cooling manifold thermal resistance within 12% of error.

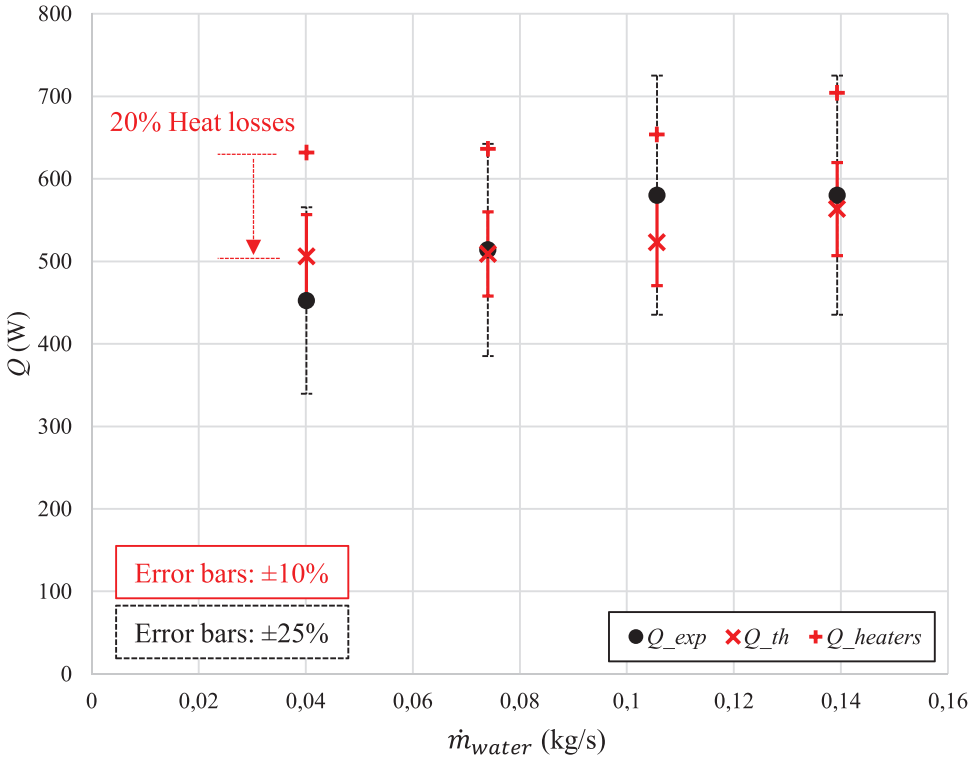

Fig. 11. Estimated and measured Heat transfer rate through the system.

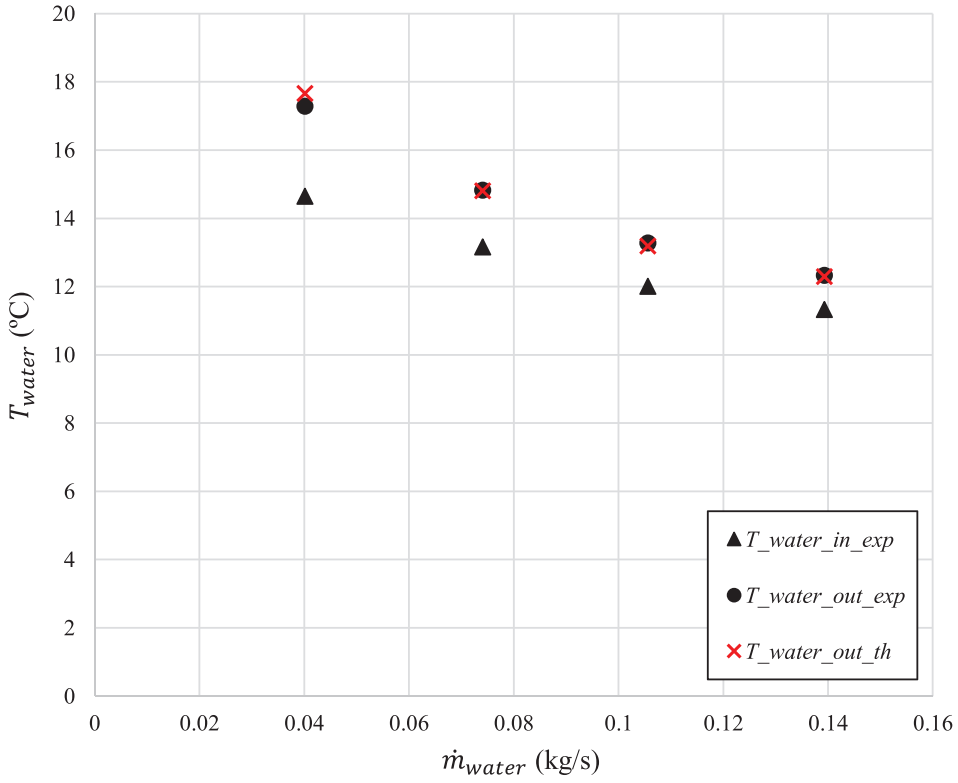

Fig. 12. Water temperature at the cooling manifold.

5.2. Heat pipe

This section focuses on the thermal behaviour of the multi-channel flat heat pipe. The temperature evolution of the multi-channel flat heat pipe with water flow rate is presented in Fig. 15 hereafter.

Because of the two-phase heat transfer taking place inside the channels of the heat pipe, the unique constant wall temperature property of a flat heat pipe is demonstrated as the temperatures LT4, RT4, LT3, RT3, RT2, SD1 and SD2 are the same for the four water flow rates tested. These temperatures are dispatched all over the heat pipe

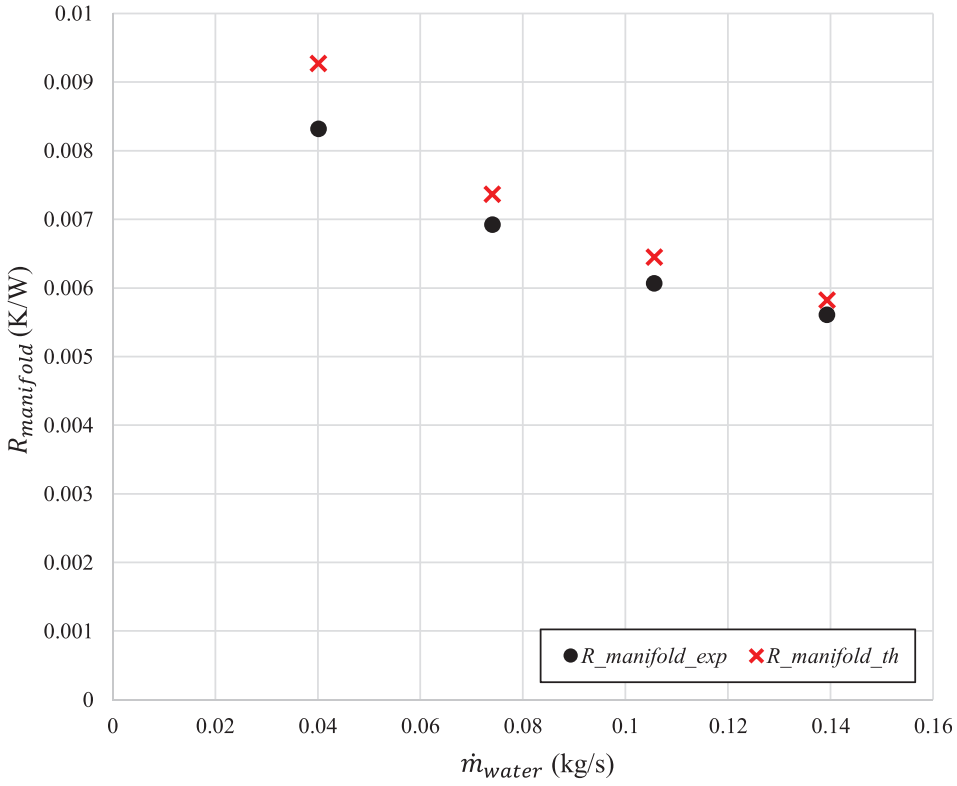

Fig. 13. Cooling manifold thermal resistance with the water flow rate.

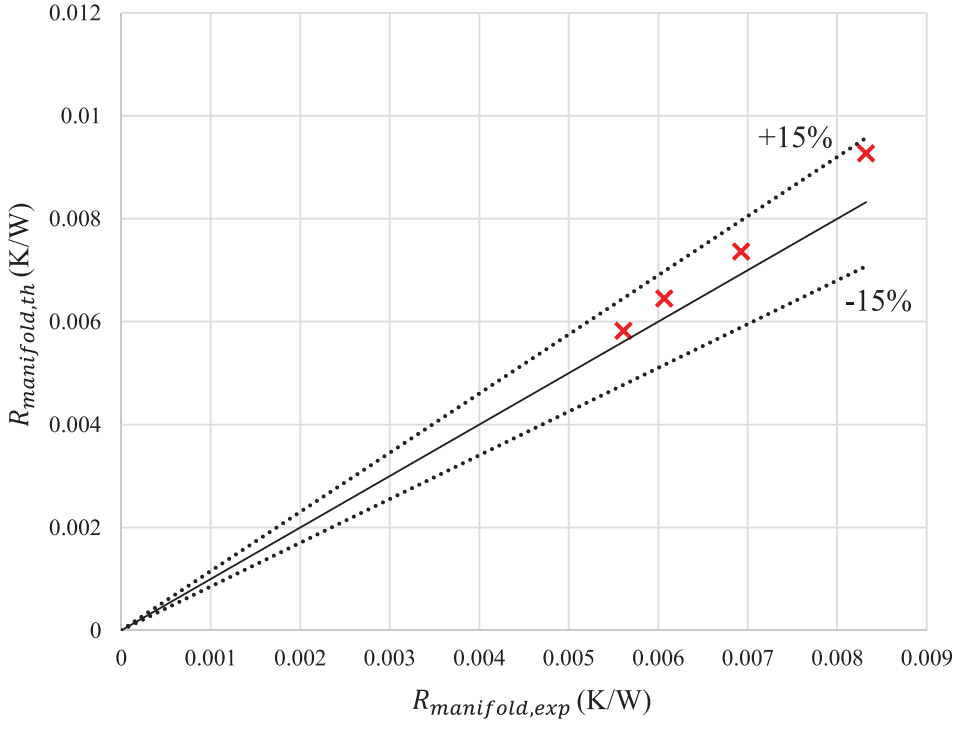

Fig. 14. Error on the cooling manifold thermal resistance estimation.

surface and highlight the cooling uniformity of the flat heat pipe surface. At the evaporator section (SD4), the surface temperature of the heat pipe is slightly higher due to the heater contact. As the electric heaters were placed on the front surface of the heat pipe, the evaporator temperature measurement (SD4) was made at the back surface of the heat pipe. At a water flow rate of 0.04 kg/s, it can be noted that a measurement error was made by the thermocouple SD4. Indeed, in a heat pipe, the evaporator temperature is higher than the adiabatic section temperature. As the seven thermocouples of the adiabatic section showed a similar temperature (maximum difference between two thermocouples of 0.3°C), the thermocouple SD4 at a mass flow rate 0.04kg/s was assumed faulty and has been replaced for the next

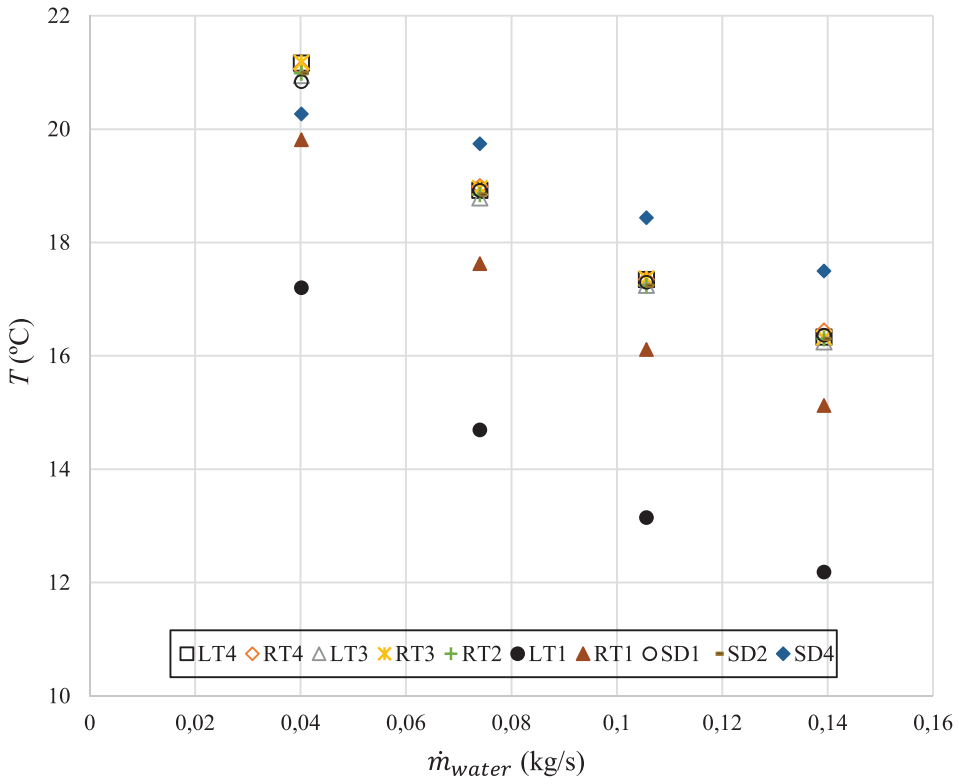

Fig. 15. Multi-channel flat heat pipe temperatures with the water flow rate.

flow rates. At the contact with the cooling manifold (RT1), the heat pipe surface temperature is lower, and condensation occurs. The temperature of the cooling manifold (LT1) is much lower due to the water flow circulating and therefore recovering the heat transmitted by the heat pipe. Hence, due to the uniform temperature profile, it seems relevant to consider a unique multi-channel flat heat pipe working temperature for each water flow rate. Experimentally, the heat pipe working temperature is determined by the heat pipe surface temperature at the adiabatic section which is the same regardless of the location as seen in Fig. 15. Generally, this temperature is close to the average between the evaporator and condenser surface temperatures. The comparison between the experimental heat pipe working temperature and the theoretical predictions made with the multi-channel flat heat pipe model developed is presented in Fig. 16.

Similar to the analysis on the cooling manifold, the multi-channel flat heat pipe working temperature predictions are in better agreement with experimental data at higher water flow rates. This is directly linked to the inaccuracies in the cooling manifold thermal resistance predictions. For instance, at a minimum water flow rate of 0.04 kg/s, an overprediction of the cooling manifold thermal resistance means more difficulties in transferring heat and therefore leads to an increase of the multi-channel flat heat pipe working temperature. Between water flow rates of 0.04 kg/s and 0.14 kg/s, the error made by the theoretical model on the working temperature prediction decreases from 6.6% to 2%. This is illustrated in Fig. 17. It is concluded that the model was able to predict the multi-channel flat heat pipe working temperature within 7% of error.

The thermal resistance of the multi-channel flat heat pipe was also estimated by the theoretical model developed by considering the two-phase heat transfer in multi-channels. The thermal resistance of a heat pipe depends on the heat transfer rate that goes through it and can vary with the tilt angle. In this study, as the heat pipe is tested vertically for all cases, only the heat transfer rate impacts the thermal resistance of the heat pipe. Indeed, the two-phase heat transfer occurring inside the channels can vary significantly according to thermal conditions imposed on the system. In this series of experiments, efforts have been made to maintain a constant heat transfer rate through the system. Experimentally, the power provided by the heaters was observed to slightly increased by 10% which may have an impact on the heat pipe thermal resistance. This analysis is presented in Fig. 18 and Table 6. To estimate the experimental thermal resistance of the multi-channel flat heat pipe, the difference of temperature between the evaporator section and the condenser section, in addition to the measured heat transfer rate recovered by the cooling manifold, are used. The evaporator temperature measurement was taken from thermocouple SD4 whereas the condenser temperature was measured according to thermocouple RT1. For a water flow rate of 0.04 kg/s, an inaccuracy in the temperature measurement is detected. This agrees with the discrepancy of the thermocouple SD4 measurement at a water flow rate of 0.04 kg/s that can be noted in Fig. 15. Therefore, this value isn't considered in the experimental and theoretical comparison for the multi-channel flat heat pipe thermal resistance.

At the studied heat transfer rates, the experimental multi-channel flat heat pipe thermal resistance was observed to be globally constant and estimated at 0.0053 K/W which is 30% higher than the measured heat pipe thermal resistance of 0.0041 K/W. It is suspected that the evaporator temperature measurements have been underestimated due to the thermocouple position at the back of the heat pipe. This has led to a smaller experimental multi-channel heat pipe resistance and thus to a higher experimental measurement error. Nevertheless, the agreement between the model and the experimental measurements is lower than 30% and is considered acceptable considering the small value of thermal resistance. Despite the promising results presented, in the current study, the number of data points remains limited and the impact of factors such as the heat transfer rate and tilt angle haven't been investigated. In this regard, at this stage, the model predictions are encouraging but the model validation is partial. To fully validate the multi-channel model presented, different heat transfer rates will be investigated in a future experiment.

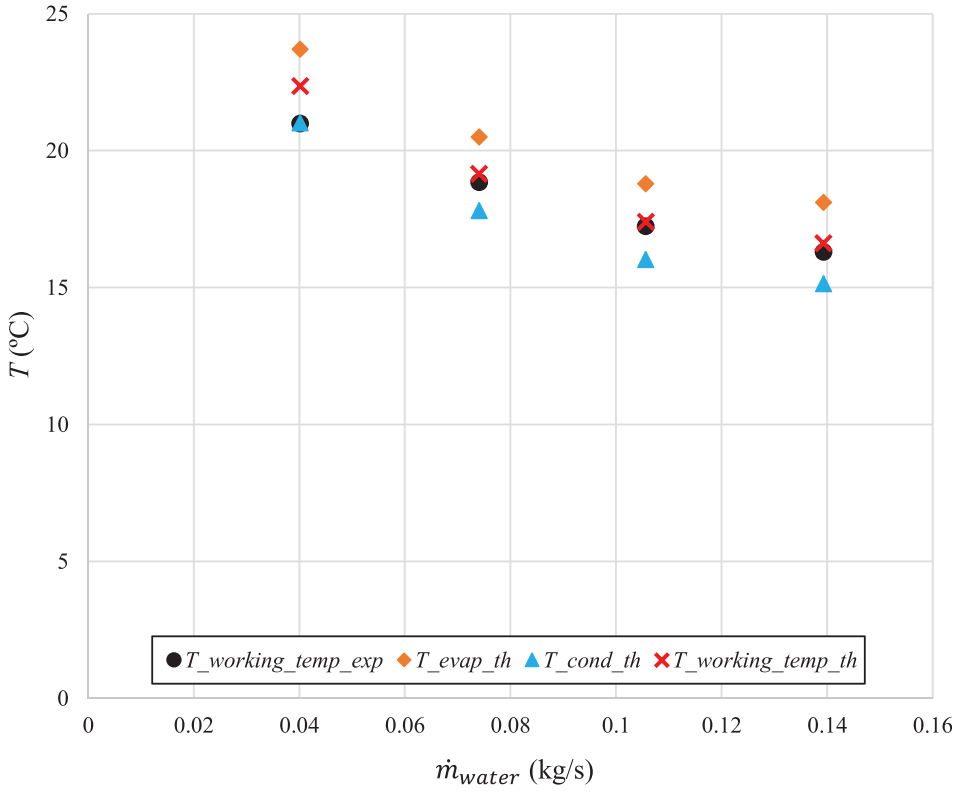

Fig. 16. Heat pipe working temperature.

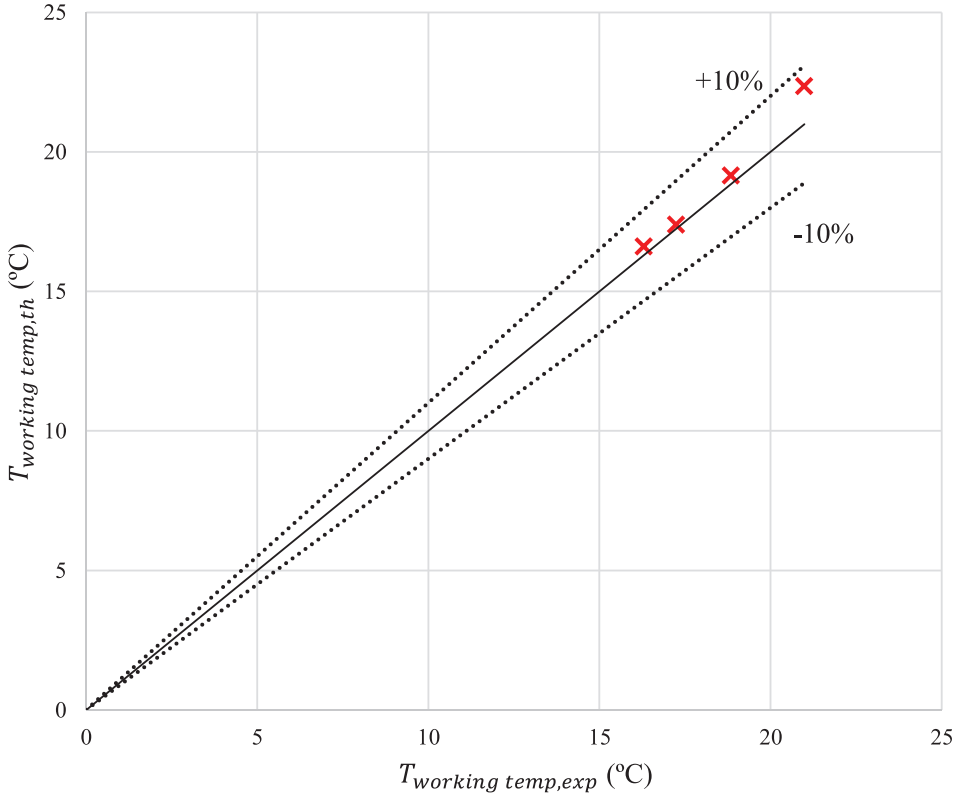

Fig. 17. Error on the heat pipe working temperature estimation.

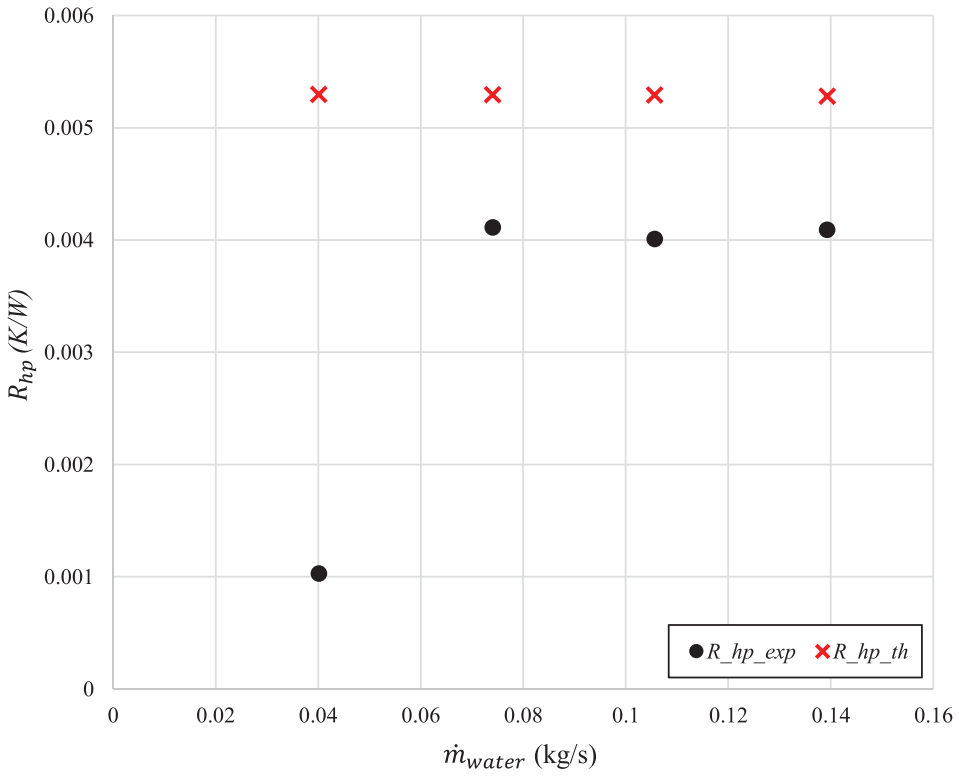

Fig. 18. Heat pipe thermal resistance.

Table 6
Error on the heat pipe thermal resistance estimation.

Flow rate (kg/s)	HP resistance – Experimental (K/W)	HP resistance – Theory (K/W)
0.07	0.00411	0.00530
0.11	0.00401	0.00529
0.14	0.00409	0.00528
Average	0.00407	0.00529
Error		29.96%

6. Conclusion

To improve the surface cooling of batteries and photovoltaic panels, the thermal performance of an innovative multi-channel flat heat pipe was investigated. In this work, the multi-channel flat heat pipe transmits thermal energy from silicon heaters to a cooling manifold in which water recovers heat by forced convection. The thermal behaviours of both the multi-channel flat heat pipe and its cooling manifold have been investigated experimentally and theoretically. This study reports a new thermal resistance model considering two-phase heat transfer in a multi-channel geometry to predict the thermal performances of the multi-channel flat heat pipe. The analytical model also considers the cooling manifold to estimate the characteristics of the complete system. Experimentally, the impact of the water flow rate on the working temperature of the heat pipe is focused. As expected, it is shown that the working temperature of the heat pipe decreases with an increase of the water flow rate. More importantly, the presented theoretical model was able to predict the water outlet temperature within 3% and the working temperature of the multi-channel flat heat pipe within 7%. The cooling manifold and multi-channel heat pipe thermal resistance have been estimated within 12% and 30% of error, respectively. The agreement between experimental data and presented multi-channel model are promising but the validation remains partial. For further model validation, impact of factors such as variable heat transfer rate and tilt angle are to be investigated.

Declaration of Competing Interest

None to declare.

Acknowledgements

This research was supported by the European project: “High-Power and High-Energy Battery Systems with Integrated Structural Thermal Management for Heavy-Duty Applications” funded by Innovate UK.

References

[1] Y.A. Cengel, Heat Transfer: A Practical Approach, McGraw-Hill, New York, 2003, pp. 785–841.
[2] H. Jouhara, et al., Experimental investigation on a flat heat pipe heat exchanger for waste heat recovery in steel industry, Energy Procedia 123 (2017) 329–334.
[3] Y. Gan, J. Wang, J. Liang, Z. Huang, M. Hu, Development of thermal equivalent circuit model of heat pipe-based thermal management system for a battery module with cylindrical cells, Appl. Therm. Eng. 164 (Jan. 2020) 114523.
[4] P. Gang, F. Huide, Z. Tao, J. Jie, A numerical and experimental study on a heat pipe PV/T system, Sol. Energy 85 (5) (May 2011) 911–921.
[5] M. Hu, R. Zheng, G. Pei, Y. Wang, J. Li, J. Ji, Experimental study of the effect of inclination angle on the thermal performance of heat pipe photovoltaic/thermal (PV/T) systems with wickless heat pipe and wire-meshed heat pipe, Appl. Therm. Eng. 106 (Aug. 2016) 651–660.
[6] Y. Deng, Z. Quan, Y. Zhao, L. Wang, Z. Liu, Experimental research on the performance of household-type photovoltaic–thermal system based on micro-heat-pipe array in Beijing, Energy Convers. Manag. 106 (Dec. 2015) 1039–1047.
[7] M. Yu, et al., Experimental Investigation of a Novel Solar Micro-Channel Loop-Heat-Pipe Photovoltaic/Thermal (MC-LHP-PV/T) System for Heat and Power Generation, Appl. Energy 256 (Dec. 2019) 113929.
[8] H. Jouhara, et al., The performance of a novel flat heat pipe based thermal and PV/T (photovoltaic and thermal systems) solar collector that can be used as an energy-active building envelope material, Energy 108 (Aug. 2016) 148–154.
[9] H. Jouhara, N. Serey, N. Khordehgah, R. Bennett, S. Almahmoud, S.P. Lester, Investigation, development and experimental analyses of a heat pipe based battery thermal management system, Int. J. Thermofluids (Nov. 2019) 100004.

[10] S. Shittu, G. Li, X. Zhao, J. Zhou, X. Ma, Y.G. Akhlaghi, Experimental study and exergy analysis of photovoltaic-thermoelectric with flat plate micro-channel heat pipe, Energy Convers. Manag. 207 (Mar. 2020) 112515.
[11] Y.H. Diao, L. Liang, Y.H. Zhao, Z.Y. Wang, F.W. Bai, Numerical investigation of the thermal performance enhancement of latent heat thermal energy storage using longitudinal rectangular fins and flat micro-heat pipe arrays, Appl. Energy 233–234 (Jan. 2019) 894–905.
[12] T. Payakaruk, P. Terdtoon, S. Ritthidech, Correlations to predict heat transfer characteristics of an inclined closed two-phase thermosyphon at normal operating conditions, Appl. Therm. Eng. 20 (9) (Jun. 2000) 781–790.
[13] H. Shabgard, B. Xiao, A. Faghri, R. Gupta, W. Weissman, Thermal characteristics of a closed thermosyphon under various filling conditions, Int. J. Heat Mass Transf. 70 (Mar. 2014) 91–102.
[14] S.H. Noie, Heat transfer characteristics of a two-phase closed thermosyphon, Appl. Therm. Eng. 25 (4) (Mar. 2005) 495–506.
[15] V. Guichet, S. Almahmoud, H. Jouhara, Nucleate pool boiling heat transfer in wickless heat pipes (two-phase closed thermosyphons): A critical review of correlations, Therm. Sci. Eng. Prog. 13 (2019).
[16] V. Guichet, H. Jouhara, Condensation, evaporation and boiling of falling films in wickless heat pipes (two-phase closed thermosyphons): A critical review of correlations, Int. J. Thermofluids (Oct. 2019) 100001.
[17] F.F. Li, Y.H. Diao, Y.H. Zhao, T.T. Zhu, J. Liu, Experimental study on the thermal performance of a new type of thermal energy storage based on flat micro-heat pipe array, Energy Convers. Manag. 112 (Mar. 2016) 395–403.
[18] B. Delpech, B. Axcell, H. Jouhara, Experimental investigation of a radiative heat pipe for waste heat recovery in a ceramics kiln, Energy 170 (Mar. 2019) 636–651.
[19] S. Almahmoud, H. Jouhara, Experimental and theoretical investigation on a radiative flat heat pipe heat exchanger, Energy 174 (May 2019) 972–984.
[20] H. Jouhara and S. Lester, "Heat Transfer Apparatus," WO2015193683, 2015.
[21] F.P. Incropera, D.P. DeWitt, T.L. Bergman, A.S. Lavine, Fundamentals of Heat and Mass Transfer, Fundam. Heat Mass Transf. (2007) 997.
[22] W.M. Rohsenow Editor, et al., Handbook of Heat Transfer, 1998.
[23] L. Prandtl, K. Ostwatitsch, K. Wieghart, Fuhrer durch die Stromungslehre, Vieweg, Braunschweig, 1944.
[24] D.K. Edwards, A.F. Mills, V.E. Denny, Transfer Processes, 2nd ed., ThriftBooks, Washington, 1979.
[25] W. M. Rohsenow, "A method of correlating heat-transfer data for surface boiling of liquids," 1952.
[26] W. Nusselt, The condensation of steam on cooled surfaces, Z. Ver. Dtsch. Ing 60 (1916) 541–546.